IEEE Access
Multidisciplinary | Rapid Review | Open Access Journal

Received April 30, 2019, accepted May 22, 2019, date of publication May 27, 2019, date of current version June 10, 2019.

Digital Object Identifier 10.1109/ACCESS.2019.2919381

An Imperceptible Medical Image Watermarking Framework for Automated Diagnosis of Retinal Pathologies in an eHealth Arrangement

BILAL HASSAN[1], RAMSHA AHMED[2], BO LI[3], AND OMAR HASSAN[4]

[1]School of Automation Science and Electrical Engineering, Beihang University (BUAA), Beijing 100191, China
[2]School of Computer and Communication Engineering, University of Science and Technology Beijing (USTB), Beijing 100083, China
[3]School of Computer Science and Engineering, Beihang University (BUAA), Beijing 100191, China
[4]Department of Electrical and Computer Engineering, Sir Syed CASE Institute of Technology (SSCIT), Islamabad 44000, Pakistan

Corresponding author: Bo Li (libo@buaa.edu.cn)

This work was supported by the National Key R&D Program of China under Grant 2017YFB0202601.

ABSTRACT The newly driven concept of electronic health (eHealth) has made distance irrelevant in healthcare. eHealth, which is commonly known as an electronic form of healthcare, refers broadly to the use of advanced information and communication technology within healthcare environments. However, its practical implementation poses many sets of challenges. One of the major challenges is authentication and integrity verification of vital medical data. Proper verification of patients with associated medical images or data is crucial to conduct accurate medical diagnostics. This paper presents an imperceptible watermarking-based security framework to address the issues of authentication and integrity verification of medical images for eHealth applications. The electronic patient record (EPR), as a watermark image, is embedded in optical coherence tomography (OCT)/fundus scan (consisting of healthy and diseased scans), using a hybrid watermarking technique based on fast curvelet transform (FCT) and singular value decomposition (SVD). The proposed work showed a high level of robustness, imperceptibility, and security for medical images when compared with the state-of-the-art existing watermarking techniques. In addition, we conducted a comparative analysis of the watermarked OCT/fundus scans with non-watermarked scans, and our results validate that the insertion of the watermark in the retinal images does not affect the automated medical image diagnosis of various retinal pathologies. Moreover, the correct recovery of the EPR from the watermarked scans makes the proposed framework applicable to the authentication of medical images for a computer-based automated diagnostic system in an eHealth arrangement.

INDEX TERMS Watermarking, medical image security, information security, electronic medical records, eHealth, fast curvelet transform, singular value decomposition, medical diagnosis, retinal pathologies.

I. INTRODUCTION

Authenticity of medical images and integrity verification of patient health information are mostly presented as important limitations in an eHealth arrangement. eHealth, which is commonly known as the electronic form of healthcare, refers broadly to the use of advanced electronic communication and information technology within healthcare environments. The digitally driven e-Health applications are the amalgamation of software and services that use the internet to record, manage and transmit medical information in a healthcare setting. eHealth can include software systems such as electronic health records or electronic medical records, which stores the electronic version of patient information such as patient's medical history, physical examination and diagnostic reports. It also includes the patient's record of treatment and investigative doctor or medical team under which the patient is treated through systematized collections, and are used by hospitals, doctors and insurance companies to record patient health information [1]. Likewise, by definition EPR refers to the electronic version of similar set of medical information about a single patient. They have not only provided a cost-effective solution to the tricky paperwork job of medical record keeping but also improved the quality of healthcare [2]. Despite the increased usefulness and espousal of electronic health and medical records, not much emphasizes is laid on the medical

The associate editor coordinating the review of this manuscript and approving it for publication was Feng Lin.

ethics considerations involved. Nevertheless, protection of patient data is undeniably one of the imperative ethical and legal issues in the field of healthcare.

Due to the sensitive nature of the information stored within electronic health records or electronic medical records, the Health Insurance Portability and Accountability Act (HIPAA) and the Health Information Technology for Economic and Clinical Health (HITECH) Act have also introduced several security safeguards to address the issues of security and confidentiality of the patient's health information, which is included in EPR [1]. HIPAA addresses these security safeguard themes for healthcare as three important pillars to secure the protected health information, labeled as administrative safeguards, physical safeguards and lastly technical safeguards. These themes range from techniques or measures regarding the usage of security equipment such as firewalls, new methods to address the issues of security and privacy of data of patients to the location of computer systems to protect the sensitive information within EPRs. Although electronic health records incorporate a large amount of health information and diagnostic data of patients, but it offers very little for the protection of this sensitive information. Moreover, the recent scientific advancements have also escalated the emergence of advanced cyber-threats and potential security breaches, such as medical data theft or stealing the patient private information are growing and dangerous crimes [2]–[4], which have put the providence of such health information systems at serious risk. Hence, there is a need to develop methods to address the issues of medical image security and privacy of patient data for eHealth applications.

A. RELATED WORK

Digital watermarking, cryptography and steganography are some of the widely used techniques for data hiding in a variety of applications for various data domains such as video, audio, image and 3D graphical objects [5], [6]. The existing research work in the field of medical image security is also based on the same data hiding techniques. In cryptography, the cover image is usually converted into an incomprehensive piece of information that is not readable, and thus it is not very encouraging in case of medical image security [7], [8]. Similarly, steganography generally does not provide strong protection against the removal or modification of hidden messages, which is again not preferred for securing medical images [9]. On the contrary, digital watermarking is recently considered a popular technique for hiding digital information in the cover signal, with maintaining the additional requirements of robustness and imperceptibility [10]–[15]. However, in the existing literature, many researchers have developed watermarking techniques for securing medical images but not much research is carried out to actually report the accuracy of medical diagnosis after the process of watermarking. Hence, there is a need to develop such watermarking techniques that not only fulfill the requirements of authenticity of medical images and integrity verification of patient health information but also yield no influence on the automated diagnosis of medical disorders from the medical images. This study proposes an imperceptible watermarking based security framework for retinal imaging modalities in automated retinal diagnostics in an eHealth setting, and storage in databases also. Imperceptible watermarking techniques can be a potential solution to solve the security issues of retinal scans in computer vision based automated diagnosis of retinal abnormalities.

B. PRELIMINARIES

Generally, based on the different applications, watermarking techniques are either categorized as fragile, semi-fragile or robust digital watermarking. While, to embed the watermark, we can either use spatial domain techniques or transform domain techniques. In the watermarking techniques based on spatial domain, the pixel values in the input media are changed directly for embedding the watermark. Whereas, in the transform domain based watermarking techniques, the watermark is embedded by changing the transform coefficients of the input media data. It is observed that, although the spatial domain watermarking techniques are computationally simple, but they offer less resistance against geometric attacks. On the contrary, transform domain watermarking techniques are more robust and less prone to various image processing and geometric attacks. Some of the common examples of watermarking techniques based on transform domain are Discrete Cosine Transform (DCT) [16], [17], Discrete Wavelet Transform (DWT) [18], Redundant Discrete Wavelet Transform (RDWT) [19], Discrete Fourier Transform (DFT) [20], Singular Value Decomposition (SVD) [18], [21] etc. In addition, hybrid-watermarking approach, using a combination of two or more transform domain techniques, is recently in practice that further improves the imperceptibility and robustness of the watermarking process [18], [21]. In our proposed study, we have used a combination of curvelet transform and SVD to develop a watermarking technique for the security of medical images.

1) FAST CURVELET TRANSFORM (FCT)

The curvelet transform is based on the theory of sparsity similar to wavelet and ridgelet transform [22]. In relative to most of the traditional transforms, curvelet transform estimates the signal to curvelet function inner relationship, and gives sparser and better representation of the signal or function. This multiscale transform also has the property of random direction selectivity, which allows it to have multiple positions and directions at every scale transforming it into a fine multiscale pyramid. With these properties curvelet transform obtains optimally sparse representation of objects, providing detailed description in nearly all the directions, with discontinuities along the edges [23]. In our proposed study, the reasons for performing watermarking based on curvelet transform is because, with its characteristic properties this scheme can bring good performance in terms of robustness and transparency. Moreover, curvelet transform allows the

watermark to be embedded or casted onto more significant positions and directions in the subbands of the image. Furthermore, it is likely to spread out the modifications across more space locations during the reconstruction of the watermark image based on the distinct transform structure of the curvelet transform. The curvelet coefficients $c(\mathcal{j}, \ell, \mathcal{k})$ [24] are expressed in Eq. (1):

$$c(\mathcal{j}, \ell, \mathcal{k}) := \left\langle x, \varphi_{\mathcal{j},\ell,\mathcal{k}} \right\rangle \tag{1}$$

Here, $\mathcal{j} = 0, 1, 2, 3 \ldots J$ represents the scale parameter, $\ell = 0, 1, 2, 3 \ldots L$ represents the orientation parameter and $\mathcal{k} = \{\mathcal{k}_1, \mathcal{k}_2\} \in \mathbb{I}$ represents the translation parameter of curvelet coefficients, respectively. Whereas, the waveform $\varphi_{\mathcal{j}}(f)$ is defined by means of its Fourier transform $\check{\varphi}_{\mathcal{j}}(\omega) = \mathcal{U}_{\mathcal{j}}(\omega)$. The frequency window $\mathcal{U}_{\mathcal{j}}$ in the Fourier domain is expressed in Eq. (2):

$$\mathcal{U}_{\mathcal{j}}(r, \theta) = 2^{\frac{-3\mathcal{j}}{4}} \left(\mathcal{W}_r\left(2^{-\mathcal{j}}\mathrm{r}\right)\right) \left(\mathcal{W}_a\left(\frac{2\left\lfloor \frac{\mathcal{j}}{2} \right\rfloor \theta}{2\pi}\right)\right) \tag{2}$$

where, $\lfloor \mathcal{j}/2 \rfloor$ represents the truncated integer of $\mathcal{j}/2$, with $\mathcal{W}_r$ and $\mathcal{W}_a$ represented as the radial and angular windows, respectively. With $2^{-\mathcal{j}}$ as scale parameter, θ_ℓ as orientation and $f_{\mathcal{k}}^{(\mathcal{j},\ell)} = \mathcal{R}_{\theta_\ell}^{-1}(k_1.2^{-\mathcal{j}}, k_2.2^{-\frac{\mathcal{j}}{2}})$ as position, the curvelet is expressed in Eq. (3):

$$\varphi_{\mathcal{j},\ell,\mathcal{k}}(f) = \varphi\left(\mathcal{R}_{\theta_\ell}\left(f - f^{(\mathcal{j},\ell)}\right)\right) \tag{3}$$

where, $\mathcal{R}_{\theta_\ell}$ represents the rotation by θ_ℓ radians and $\theta_\ell = 2\pi(\ell(2^{-\lfloor \mathcal{j}/2 \rfloor}))$. Further, $\ell = 0, 1, 2, 3 \ldots L$ and $0 \leq \theta_\ell < 2\pi$.

2) SINGULAR VALUE DECOMPOSITION (SVD)

SVD is a numerical analysis tool that is used widely in many applications related to image processing. Lately, many hybrid-watermarking techniques are being developed, where SVD is used along with other transform domain techniques to build a more robust and imperceptible watermarking process [18], [21]. One major advantage of using SVD is that, it is very resistant to most of the image processing attacks. Where, although the singular values might be mostly affected, still it substantially preserves the overall integrity of the data. Moreover, SVD provides good stability and even with the addition of minor perturbations, no significant changes are observed in the singular values of the input data upon reconstruction [25]. SVD is expressed in Eq. (4-5):

$$I = \mathcal{u} \times \mathcal{s} \times \mathcal{v}' \tag{4}$$

$$I = \begin{bmatrix} \mathcal{u}_{1,1} & \cdots & \mathcal{u}_{1,n} \\ \vdots & \ddots & \vdots \\ \mathcal{u}_{n,1} & \cdots & \mathcal{u}_{n,n} \end{bmatrix} \times \begin{bmatrix} \mathcal{s}_{1,1} & \cdots & 0 \\ \vdots & \ddots & \vdots \\ 0 & \cdots & \mathcal{s}_{n,n} \end{bmatrix} \times \begin{bmatrix} \mathcal{v}_{1,1} & \cdots & \mathcal{v}_{1,n} \\ \vdots & \ddots & \vdots \\ \mathcal{v}_{n,1} & \cdots & \mathcal{v}_{n,n} \end{bmatrix}' \tag{5}$$

where, $\mathcal{u}$ and $\mathcal{v}$ represent the orthogonal matrices of I, and $\mathcal{s}$ represents the diagonal matrix of I, with non-negative singular values arranged in a descending order. In our study, we have proposed a hybrid watermarking technique based on the combination of curvelet transform and SVD to build a more robust and imperceptible watermarking process. The characteristic properties of both curvelet transform and SVD as mentioned earlier provide more transparency and robust extraction of watermark for medical image security.

3) FALSE POSITIVE PROBLEM IN SVD AND SOLUTION

One of the most vital and crucial application of robust watermarking is the rightful protection of digital media ownership. Ideally, an efficient watermarking scheme should aim for the protection of rightful owners through copyright protection and authentication, and only the real owners should be able to extract the embedded watermark from the watermarked images correctly, to prove their ownership. However, due to the recent increase in the security and privacy breaches in content ownership and unauthorized access, an attacker can embed an illegal watermark in the same digital media that is watermarked by its real owner and then claim the possible ownership of the media contents after extracting the illegal watermark contents. This situation can present a very critical security concern for the real owners of the media contents in proving their rightful ownership. Hence, such kind of challenges are referred as False Positive Problem (FPP) in watermarking schemes, where an illegal or non-embedded watermark can be extracted from the host images to ascertain the false ownership [25].

Generally, SVD based watermarking techniques are very stable and satisfy the criteria of robustness and transparency quiet efficiently. In SVD, a matrix is decomposed into singular values, consisted on three matrices: $I = \mathcal{u} \times \mathcal{s} \times \mathcal{v}'$, where $\mathcal{s}$ represents the diagonal singular values and $\mathcal{u}$ and $\mathcal{v}$ represent the left and right singular vectors. The details of SVD are mentioned in section SVD. However, it is observed that when watermark embedding is performed in $\mathcal{s}$ vector of the SVD domain, even due to its characteristic properties and stability such schemes are subjected to high probability of FPP [25], [26]. Commonly, researchers adopt two methods to embed the watermark in $\mathcal{s}$ vector of the SVD domain: (i) embedding the watermark bits directly in the singular values of the host image, as shown in Figure 1(a) or (ii) embedding the singular values of the watermark in the singular values of the host image, as shown in Figure 1(b). While, the left and right singular vectors are passed as secret information during the watermark extraction process. These methods are vulnerable to FPP problem because, $\mathcal{s}$ vector represent only the luminance and does not carry any vital information about the host image, whereas, on the other hand $\mathcal{u}$ and $\mathcal{v}$ singular vectors, which are passed as secret information during watermark extraction, represent important data about the host image such as its geometric properties and features of the image structure. Therefore, an attacker, using this vulnerability of the SVD domain based watermarking schemes, can pass forged singular vectors as secret information during the watermark extraction process to obtain a new

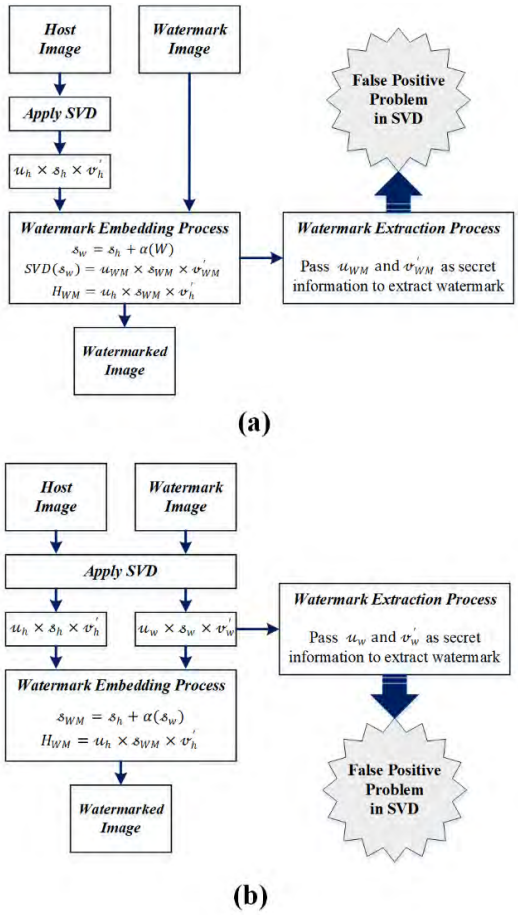

FIGURE 1. Common practices leading to FPP in SVD based watermarking. (a) Case I. (b) Case II.

forged watermark. In this way, an attacker can successfully claim the false ownership of the image irrespective of the extracted singular values during the watermark extraction process [25].

To solve the problem of FPP in SVD, we have implemented two solutions in our proposed study. First, we embedded the watermark bits using the singular values in u left vector instead of s diagonal singular vector of the host image. While, during the watermark extraction process, only the entries in u singular vector of the host-watermarked image are examined to recover the watermark bits and no secret or side information (s and v singular vectors) is passed on for extracting the watermark. This strategy of embedding the watermark solves the vulnerability in SVD as mentioned earlier and eliminates the FPP problem altogether. Secondly, before embedding, the watermark is encrypted using a Private Secret Key (PSK) known only to the ophthalmologist. Therefore, after extracting the watermark, it is required to be decrypted using the same PSK to recover the true watermark. This adds another layer of data security against the false ownership claims and unauthorized access of the watermark by attackers.

C. OVERVIEW OF RETINAL IMAGING MODALITIES AND PATHOLOGIES USED IN THIS STUDY

In this study, we have used two types of retinal imaging modalities to generate watermarked scans and study the influence of watermark embedding for automated diagnosis of various retinal abnormalities. These imaging modalities are mainly OCT and fundus photography. OCT is relatively new eye examination technique introduced first in 1993 [27]. It is a non-invasive mean of acquiring cross-sectional view of human retina. The major advantage with OCT over other retinal imaging modalities is that symptoms of various retinal syndromes appear in the early stages which are not visible in other imaging modalities. This leads to timely treatment of eye disorders to avoid escalation of disease, which may result in blindness. On the other hand, fundus photography also known as Fluorescein Angiography (FA) captures the inner structures of human eye such as central and peripheral retina, optics disc and macula region [28]. It is another non-invasive eye examination technique used to treat macular pathologies. The benefit of fundus photography is that it can detect maculopathy easily especially in diabetic patients.

Macular Edema (ME) and Central Serous Chorioretinopathy (CSCR) are two common macular disorders, which greatly affect the central vision in a patient. Diabetic patients are more prone to develop ME, where blood capillaries in macula region get ruptured and start to leak cystoid fluid. This accumulation of cystoid fluid swells the macula region leading to central vision loss. While, CSCR is another macular condition in which retinal layers are detached due to the deposition of serous fluid beneath the retina [29]. In the proposed study, both watermarked OCT and fundus scans are analyzed to automatically diagnose these two macular disorders using machine learning approach.

Considering OCT scans, healthy OCT scan shows that the retinal layers are well intact without any deposition of cystoid fluid. In addition, the fovea is located at the minimum separation between Nerve Fiber Layer (NFL) and Retinal Pigment Epithelium (RPE) layer. On the contrary, ME affected OCT scan shows visible cystic spaces between the retinal layers due to deposition of cystoid fluid and increased separation between NFL and RPE at fovea. Likewise, CSCR affected OCT scan shows the accumulation of serous fluid beneath the retina resulting in detachment of retinal layers and fovea dislocation. Figure 2(a) shows the OCT scans of healthy, ME and CSCR affected eyes respectively, where cystoid fluid and foveal thickness are indicated in each case. In fundus scans, heathy fundus scan does not contain blisters of fluid and hard exudates in macula region. Whereas, the macula region shows presence of hard exudates and fluid blisters in both cases of ME and CSCR affected fundus scans. Figure 2(b) shows the fundus scans of healthy, ME and CSCR affected eyes respectively, where optic disc, blood vessels, macula region, hard exudates and blisters of fluid are indicated in each case. Rest of the paper is organized as: section II explains the proposed framework, experimental results are presented

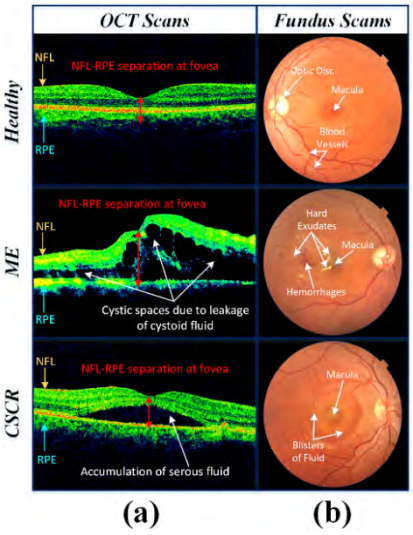

FIGURE 2. Retinal pathologies and symptoms. (a) Visualization via OCT scans. (b) Visualization via fundus scans.

in section III, followed by discussion in section IV. Section V concludes the paper with scope of future work.

II. PROPOSED FRAMEWORK

Medical image security and privacy of patient data are becoming critical and growing issues for eHealth applications. However, watermarking being a potential solution can serve the purpose of authentication and integrity verification of medical images and EPR before a patient's medical diagnosis or treatment. It is also important to ensure that the watermarked medical images should be highly imperceptible after the embedding of watermark, as they are to be used for medical diagnosis of patients by doctors. Therefore, watermark embedding is a comparatively critical task in the medical images than natural images. Moreover, it requires robust extraction of watermark contents to confirm proper authentication and integrity verification. This paper presents a security framework based on watermarking algorithm, using FCT and SVD to secure medical images by embedding the associated EPR in the medical image, with maintaining the overall perceptual transparency and integrity of the patient medical and private data. Figure 3 gives the detailed block diagram of our proposed framework for retinal image security and authentication with patient health information in the form of EPR. Additionally, the framework is designed to perform uncompromised automated diagnosis of various retinal pathologies using the watermarked OCT and fundus scans. The proposed framework consists of four main stages as following:

A. PATIENT COMPREHENSIVE EYE EXAM

Secure watermarked retinal scan in our framework is generated through two images, original OCT/fundus scan of the patient and the patient private information in the form

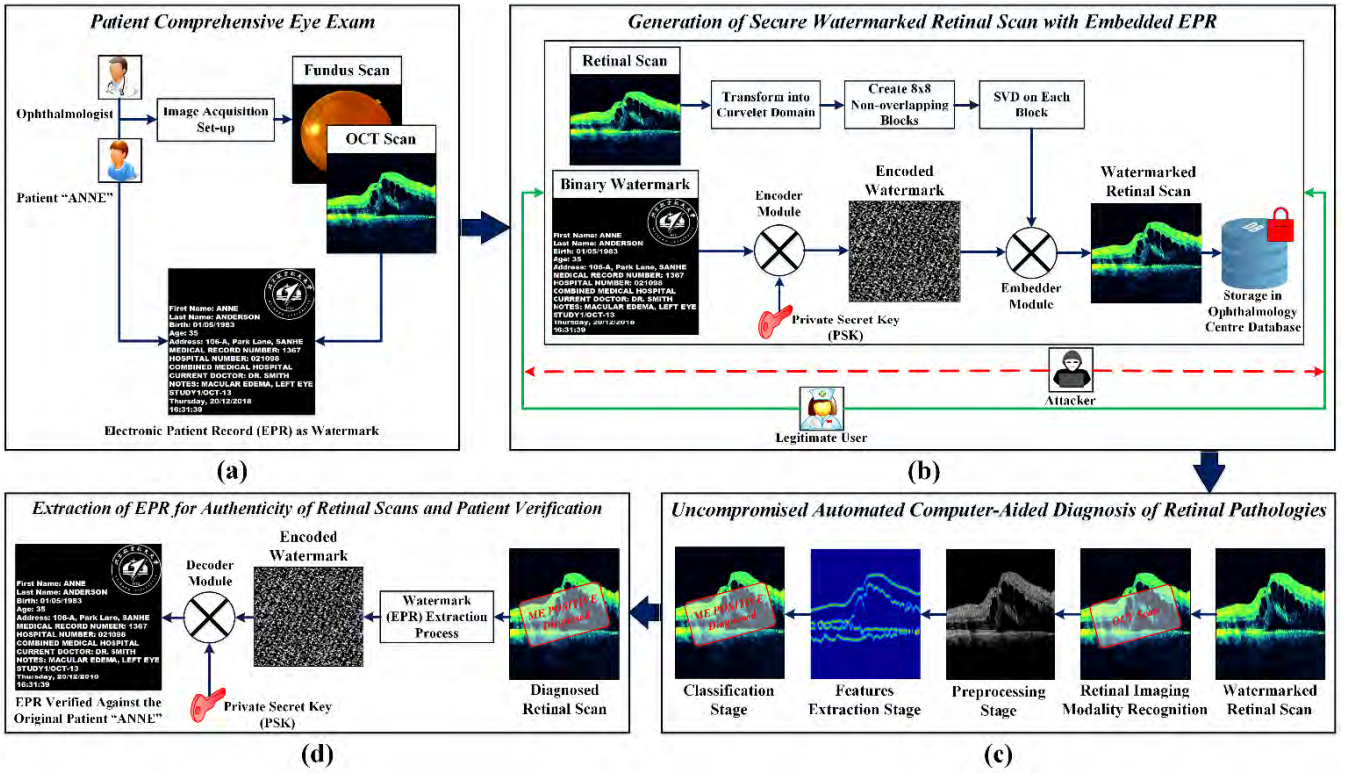

FIGURE 3. Proposed framework. (a) Patient comprehensive eye exam. (b) Generation of secure watermarked retinal scan with embedded EPR. (c) Uncompromised automated computer-aided diagnosis of retinal pathologies. (d) Extraction of EPR for authenticity of retinal scans and patient verification.

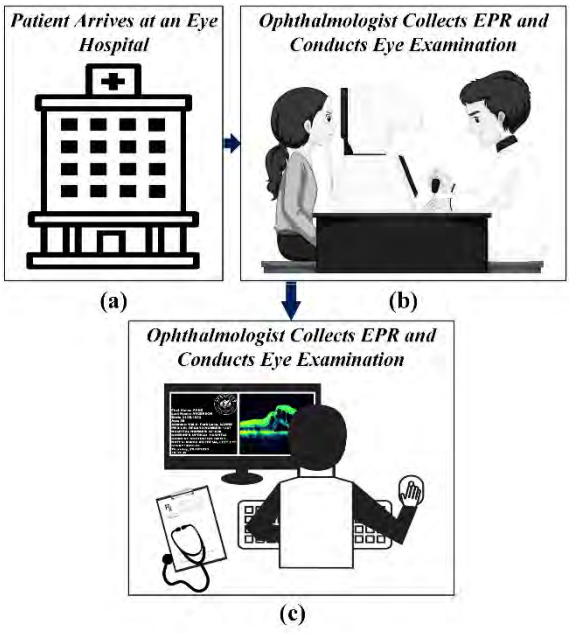

FIGURE 4. Patient comprehensive eye exam. (a) Patient arrives at an eye hospital. (b) Ophthalmologist collects EPR and conducts eye examination. (c) Ophthalmologist records retinal scans with EPR in the system.

of EPR. This information is subsequently collected in the first stage of our framework by ophthalmologists as shown in Figure 4. When a patient arrives at a hospital or clinic for checkup, initially ophthalmologist will conduct a comprehensive eye exam of the patient using the retinal scan acquisition machines. In the process ophthalmologist records the patient OCT and fundus scans along with patient EPR in the system.

B. GENERATION OF SECURE WATERMARKED RETINAL SCAN WITH EMBEDDED EPR

Once the ophthalmologist collects and records the patient medical information in the form of OCT/fundus scans and EPR, the system is ready to move forward with the second stage of secure watermarked retinal scan generation. This stage comprises of two steps: (i) Watermark (EPR) encoding and (ii) Watermark (EPR) embedding. The block diagrams and detailed explanation of these steps are as following:

1) WATERMARK (EPR) ENCODING

Let $\mathcal{R}_{OS}$ be the original retinal scan and ω_{EPR} be the binary watermark image of EPR, of $P \times Q \times R$ and $X \times Y$ dimensions, respectively. Here, $p = 1, 2, 3, \ldots P$ represents the rows, $q = 1, 2, 3, \ldots Q$ represents the columns and $r = 1, 2, 3$ represents the color bands of original retinal scan. Similarly, $x = 1, 2, 3, \ldots X$ represents the rows and $y = 1, 2, 3, \ldots Y$ represents the columns of the watermark EPR image used. Table 1 shows the parameters of the host and watermark images used in our study. Since, the original retinal scans are of different sizes as evident from Table 1, we first normalized $\mathcal{R}_{OS}$ to 512×512 dimensions to match with the size of watermark.

TABLE 1. Host and watermark image parameters.

Host Image ($\mathcal{R}_{OS}$) ($P \times Q \times R$)		Watermark Image (ω_{EPR}) ($X \times Y$)
OCT Scans	Fundus Scans	
512 × 496 (2D 8 bit grayscale) 768 × 496 (2D 8 bit grayscale) 480 × 1280 × 3	2032 × 1934 × 3	512 × 512 (Binary Image)

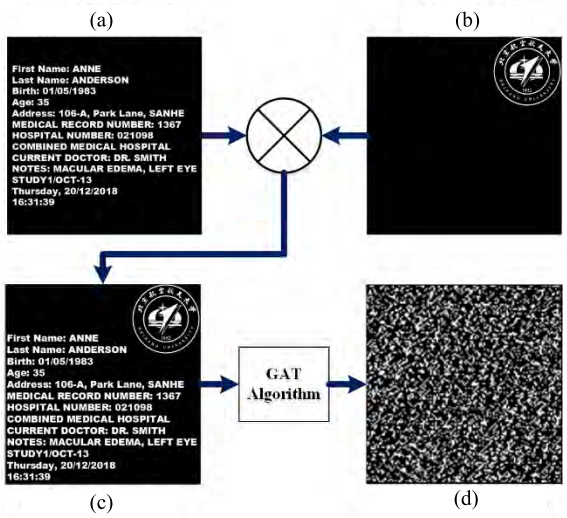

FIGURE 5. Encoded watermark image generation. (a) Hospital/clinic logo ($\omega(x, y)$). (b) EPR ($EPR(x, y)$). (c) Fused watermark image($\omega_{EPR}(x, y)$). (d) Encoded watermark ($\tilde{\omega}_{EPR}(\acute{x}, \acute{y})$).

The final watermark image $\omega_{EPR}(x, y)$ used in this proposed study is generated using fusion of two images. One is the hospital/clinic logo ($\omega(x, y)$), to serve the purpose of its medical record ownership and authentication and second is the EPR ($EPR(x, y)$), collected and recorded by ophthalmologist to verify the patient identity under diagnosis or treatment, respectively, as shown in Figure 5.

Also, before embedding the EPR, Generalized Arnold Transform (GAT) algorithm is applied on the watermark image to transform it into an encoded watermark image $\tilde{\omega}_{EPR}(\acute{x}, \acute{y})$ as shown in Figure 5(d), using a Private Secret Key (PSK) known only to the ophthalmologist treating the patient and the authorized hospital/clinic staff under the ophthalmologist. Each ophthalmologist uses his or her own unique private secret key for this purpose. This adds an extra layer of security and protects the patient information from unauthorized access or use. The GAT algorithm is expressed in Eq. (6-7):

$$\begin{bmatrix} \acute{x} \\ \acute{y} \end{bmatrix} = \Lambda^{i} \begin{bmatrix} x \\ y \end{bmatrix} (mod\ S) \tag{6}$$

$$\Lambda = \begin{bmatrix} 1 & 1 \\ K & K+1 \end{bmatrix} \tag{7}$$

where, Λ represents the GAT algorithm, x, y, $\acute{x}$ and $\acute{y}$ are the location of the pixels in the watermark image before and after

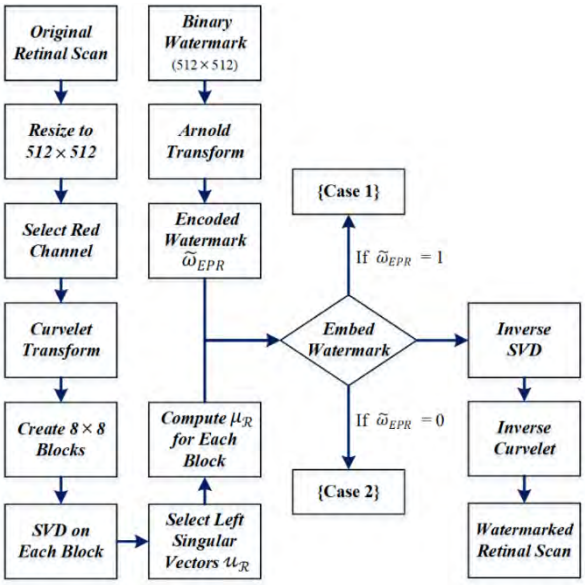

FIGURE 6. Block diagram of Curvelet and SVD based watermark embedding.

GAT is applied, respectively. i is the number of iterations, K represents the private secret key and S represents the size of the watermark EPR image i.e. 512 × 512.

2) WATERMARK (EPR) EMBEDDING

In the proposed study, the encoded EPR $\tilde{\omega}_{EPR}(\acute{x}, \acute{y})$ is embedded in the original retinal scan $\mathcal{R}_{OS}(p, q)$ using a hybrid watermarking technique based on FCT and SVD transforms. Load the input color OCT/ fundus scan into the system and rescale it to a dimension of 512 × 512 to match the size of the binary watermark EPR image. The binary watermark is encoded using the Arnold transform to generate the encoded watermark. First, extract the red channel from the input RGB image. In the next step, apply curvelet transform to decompose the red channel and generate an array of complex curvelet coefficients using a threshold value. Then, combine these complex coefficients in the form of a curvelet image. At this point, divide the curvelet image to non-overlapping blocks of 8 × 8 size for watermark embedding. Then, apply SVD on each block to get the singular values. Using only the left singular vector $u_{\mathcal{R}}$, embed the encoded watermark bits by examining the entries based on another threshold value. After modifying the $u_{\mathcal{R}}$ matrix entries in each block, apply inverse SVD to get the modified blocks of curvelet image. Then, apply inverse curvelet transform to reconstruct the modified red component, and concatenate with green and blue channels to generate the watermarked OCT/ fundus scan $\mathcal{R}_{WS}(p, q)$ for storage in the ophthalmology center databases. Figure 6 and Algorithm 1 shows the detailed curvelet and SVD based watermark embedding process used in our proposed study.

Algorithm 1: Watermark Embedding Process

1 Load the original OCT/ fundus scan $\mathcal{R}_{OS}(p, q)$ and resize to 512 × 512 dimensions to match the size of the binary watermark (512 × 512)
2 Apply Arnold transform to encode the binary watermark $\omega_{EPR}(xy)$
3 Extract and select the red channel out of input RGB scan for embedding the encoded watermark $\tilde{\omega}_{EPR}(\acute{x}\acute{y})$
4 Define threshold T'; apply curvelet transform to generate a curvelet image of complex curvelet coefficients; $\mathcal{C}_{\mathcal{R}}(\acute{j}\acute{\imath}) := \sum_{0\le t_1,t_2<n} \rho[t_1, t_2]\varphi_{\acute{j}\acute{\imath}}.[\bar{t}_1, t_2]$ from the selected red channel
5 Divide the curvelet image into non-overlapping blocks of 8 × 8 size i.e. $\sum_{R=1}^{n}[\beta_{\mathcal{R}}(p, q)]$, where n is the total number of non-overlapping blocks
6 Apply SVD (Δ) on each block $\beta_{\mathcal{R}}(pq)$ to obtain the singular values for each block i.e. $[u_{\mathcal{R}}\ \jmath_{\mathcal{R}}\ v_{\mathcal{R}}] = \Delta[\beta_{\mathcal{R}}(pq)]$
7 Define threshold T''; only examine the entries in $u_{\mathcal{R}}$ matrix of each block for embedding the encoded watermark
8 Select the first eight entries in $u_{\mathcal{R}}$ that have the lowest values in each block and compute $\mu_{\mathcal{R}} = \frac{\left\{\left|u^1_{i,\acute{j}}\right|+\left|u^2_{i,\acute{j}}\right|+\ldots+\left|u^8_{i,\acute{j}}\right|\right\}}{8}$, where $u_{i,\acute{j}} \in u_{\mathcal{R}}$
for $\acute{k} = 1 : M$ % Where M is the size of the watermark%
  if $\tilde{\omega}_{EPR}(\acute{k}) == 1$ %{CASE 1}%
  then
    $u^1_{i,\acute{j}} = \mu_{\mathcal{R}} + \frac{T''}{2}$;
    $u^2_{i,\acute{j}} = \mu_{\mathcal{R}} - \frac{T''}{2}$;
    ⋮
    $u^8_{i,\acute{j}} = \mu_{\mathcal{R}} - \frac{T''}{2}$;
  else
    $\tilde{\omega}_{EPR}(\acute{k}) == 0$ %{CASE 2}%
    then
    $u^1_{i,\acute{j}} = \mu_{\mathcal{R}} - \frac{T''}{2}$;
    $u^2_{i,\acute{j}} = \mu_{\mathcal{R}} + \frac{T''}{2}$;
    ⋮
    $u^8_{i,\acute{j}} = \mu_{\mathcal{R}} + \frac{T''}{2}$;
  end
end
9 Apply inverse SVD (∇) using each modified $\check{u}_{\mathcal{R}}$ matrix; $\check{\beta}_{\mathcal{R}}(pq) = \nabla[\check{u}_{\mathcal{R}} * \jmath_{\mathcal{R}} * v^T_{\mathcal{R}}]$ to get the modified 8 × 8 size blocks i.e. $\sum_{R=1}^{n}[\check{\beta}_{\mathcal{R}}(p, q)]$, where n is the total number of non-overlapping modified blocks
10 Apply inverse curvelet transform on the modified blocks to reconstruct the modified red component, and concatenate with green and blue channels to generate the watermarked image $\mathcal{R}_{WS}(pq)$

C. UNCOMPROMISED AUTOMATED COMPUTER-AIDED DIAGNOSIS OF RETINAL PATHOLOGIES

After the successful creation of watermarked retinal scans of patients, the third stage of our proposed framework is automated diagnosis of retinal pathologies. We evaluated these watermarked retinal scans against our existing machine learning based algorithms to automatically classify various

retinal pathologies such as ME, CSCR etc. The aim of this stage is to evaluate if the insertion of watermark (EPR) in the original retinal scans affects the outcome of automated diagnostic system and to check the transparency of watermark. For this purpose, we used our existing automated retinal diagnostic systems against the watermarked retinal scans and compared the results. The detailed implementation and working of these algorithms can be referred in articles [29]–[33]. It is pertinent to mention here that this stage is irrespective of the embedding and extraction of watermark and only performs the automated diagnosis of retinal pathologies using the watermarked retinal scans. The working model for automated classification of retinal pathologies using machine learning approach, is briefly explained as following: (i) First, input retinal modality (i.e. watermarked OCT/fundus scan) is recognized using machine learning techniques. (ii) The next step is preprocessing, in which the input retinal scan is denoised and the most meaningful information is extracted for further processing. (iii) After that, 2-Dimensional (2-D) structure tensor approach is used to compute distinguished features between different retinal pathologies. (iv) Once the features are extracted, they are passed to supervised machine learning classifiers for training and classification of various retinal pathologies in the final step. Figure 7 shows the process of uncompromised automated diagnosis of retinal pathologies from the watermarked scans.

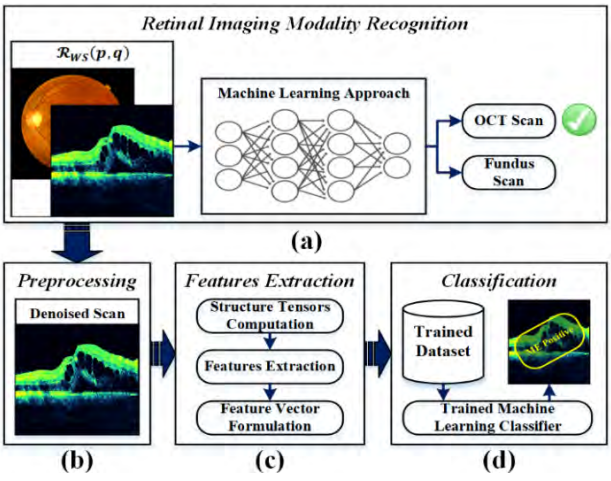

FIGURE 7. Uncompromised automated computer-aided diagnosis of retinal pathologies. (a) Retinal imaging modality recognition. (b) Preprocessing. (c) Features extraction. (d) Classification.

The watermarked retinal scan ($\mathcal{R}_{WS}(p, q)$) after embedding EPR, is fed to this stage, where it predicts the outcome and labels the scan as "Diagnosed Retinal Scan" (ME positive, CSCR positive or healthy), as shown in Figure 3 of this paper. Moreover, this diagnosed retinal scan is same as the watermarked retinal scan, which in turn is passed to the next stage to recover the embedded EPR.

D. EXTRACTION OF EPR FOR AUTHENTICITY OF RETINAL SCANS AND PATIENT VERIFICATION

In the final stage of our proposed framework, the information that was embedded in the retinal scans to ensure the privacy of patient medical and private data is extracted for verification purposes. In order to extract the embedded watermark (EPR) from the watermarked retinal scan $\mathcal{R}_{WS}(p, q)$, the process of extraction works exactly in the reverse order of the embedding. By inversing the steps, the encoded EPR $\tilde{\omega}_{EPR}(\acute{x}, \acute{y})$ is obtained. Next, to decode the true information for authenticity and integrity verification of retinal scans and patient identification, ophthalmologist uses the same unique PSK, which he or she used initially to secure this information.

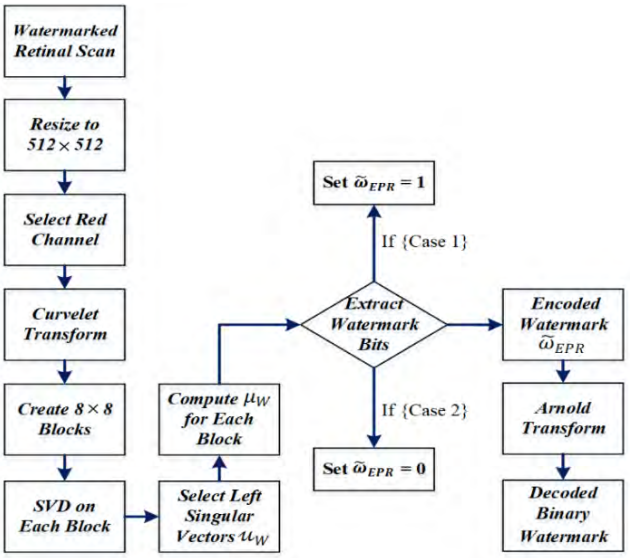

FIGURE 8. Block diagram of Curvelet and SVD based watermark extraction.

1) WATERMARK (EPR) EXTRACTION

First, load the watermarked color OCT/ fundus scan $\mathcal{R}_{WS}(p, q)$ and extract the red channel. Then, apply curvelet transform on the extracted red channel to obtain the watermarked curvelet image. In the similar manner, divide this image to 8 × 8 non-overlapping blocks, now for watermark extraction. In the next step, apply SVD on each block and obtain the watermarked left singular vectors u_W. Then, based on the entries in each u_W matrix for each block recover the encoded watermark bits as zero or one, using the same threshold value as used in the watermark embedding process. After that, these extracted watermark bits are rearranged and decoded using the Arnold transform to recover the binary watermark image $\omega_{EPR}(x, y)$. Figure 8 and Algorithm 2 shows the detailed curvelet and SVD based watermark extraction process used in our proposed study.

III. EXPERIMENTAL RESULTS AND ANALYSIS

This section discusses the experimental results of our proposed study. The reported results show that the proposed

Algorithm 2: Watermark Extraction Process

1 Load the watermarked OCT/ fundus scan $\mathcal{R}_{WS}(pq)$ and resize to 512 × 512 dimensions
2 Extract and select the red channel out of input RGB scan for extracting the encoded watermark
3 Define threshold T'; apply curvelet transform to generate a watermarked curvelet image of complex curvelet coefficients from the selected red channel
4 Divide the watermarked curvelet image into non-overlapping blocks of 8 × 8 size i.e. $\sum_{W=1}^{n}[\beta_W(p,q)]$, where n is the total number of non-overlapping watermarked blocks
5 Apply SVD (Δ) on each watermarked block $\beta_W(pq)$ to obtain the singular values for each block i.e. $[\mathcal{u}_W\ \mathcal{s}_W\ \mathcal{v}_W] = \Delta[\beta_W(pq)]$
6 Define threshold T''; only examine the entries in watermarked $\mathcal{u}_W$ matrix of each block for extracting the encoded watermark
7 Select the first eight entries in $\mathcal{u}_W$ that have the lowest values in each block and compute $\mu_W = \frac{\left\{\left|u^1_{i,\mathcal{J}}\right|+\left|u^2_{i,\mathcal{J}}\right|+\ldots+\left|u^8_{i,\mathcal{J}}\right|\right\}}{8}$, where $\mathcal{u}_{i,\mathcal{J}} \in \mathcal{u}_W$
8 Each bit of watermark is recovered from each block as following:
for $k = 1 : M$ % Where M is the size of the watermark%
  if $u^1_{i,\mathcal{J}} == \mu_W + \frac{T''}{2}$ %{CASE 1}%
    && $u^2_{i,\mathcal{J}} == \mu_W - \frac{T''}{2}$
    ⋮
    && $u^8_{i,\mathcal{J}} == \mu_W - \frac{T''}{2}$
    then $\omega_{EPR}(\hbar) = 1$;
  else
    $u^1_{i,\mathcal{J}} == \mu_W - \frac{T''}{2}$ %{CASE 2}%
    && $u^2_{i,\mathcal{J}} == \mu_W + \frac{T''}{2}$
    ⋮
    && $u^8_{i,\mathcal{J}} == \mu_W + \frac{T''}{2}$
    then $\omega_{EPR}(\hbar) = 0$;
  end
end
9 The extracted watermark bits are then rearranged and decoded using the Arnold transform to recover the binary watermark image $\omega_{EPR}(x, y)$

watermarking based security framework successfully maintains the overall perceptual transparency and integrity of the patient medical and private data for eHealth applications. Additionally, this section includes various comparative studies based on our existing machine learning algorithms to show that the proposed framework does not influence but facilitates uncompromised automated retinal diagnostics, including diagnosis of retinal pathologies (such as ME and CSCR), using original and watermarked OCT/fundus scans.

TABLE 2. Dataset details.

Algorithm	8-bit Retinal Imaging Modality	Resolution(s)	Healthy	ME	CSCR
[29], [30], [31], [32]	OCT scans	512×496 768×496 480×1280	165	116	110
[33]	Fundus scans	2032×1934	40	31	-

A. DATASET DETAILS

The dataset used in this study includes OCT and fundus scans of different retinal pathologies such as healthy, ME and CSR. We acquired the datasets from two publicly available sources, (i) BioMedical Image and Signal Analysis (BIOMISA) dataset [34] and (ii) Duke dataset [35]. The details of both datasets that we used for validation of our results are shown in Table 2.

B. PERFORMANCE METRICS FOR ROBUSTNESS AND IMPERCEPTIBILITY CHECK OF WATERMARK

To investigate the performance of the proposed watermarking scheme in terms of imperceptibility and robustness against various image processing and geometric attacks, we have used the following metrics:

1) PEAK SIGNAL TO NOISE RATIO (PSNR)

Imperceptibility or transparency is defined as the measure of similarity between the host $\mathcal{I}_{i,\mathcal{J}}$ and watermarked $\bar{\mathcal{I}}_{i,\mathcal{J}}$ images and it is measured through PSNR. PSNR is expressed in Eq. (8):

$$PSNR(\mathcal{I}, \bar{\mathcal{I}}) = 10\log 10\frac{max\left(\mathcal{I}_{i,\mathcal{J}}\right)^2}{MSE} \tag{8}$$

Here, $max\left(\mathcal{I}_{i,\mathcal{J}}\right)$ represents the maximum value of pixel in the host image. Whereas, Mean Square Error (MSE) between the host and watermarked image is expressed in Eq. (9):

$$MSE = \frac{1}{m \times n}\sum_{i=1}^{m}\sum_{\mathcal{J}=1}^{n}\left[\mathcal{I}_{i,\mathcal{J}} - \bar{\mathcal{I}}_{i,\mathcal{J}}\right]^2 \tag{9}$$

where, $m \times n$ represent the dimensions of host and watermarked images.

2) STRUCTURAL SIMILARITY INDEX (SSIM)

In addition to PSNR, we have used another metric i.e. SSIM to measure the imperceptibility between the host $\mathcal{I}_{i,\mathcal{J}}$ and watermarked $\bar{\mathcal{I}}_{i,\mathcal{J}}$ images. SSIM also measures the similarity between these two images based on the comparative measurements of three individual parameters: luminance $\ell\left(\mathcal{I}, \bar{\mathcal{I}}\right)$, contrast $c\left(\mathcal{I}, \bar{\mathcal{I}}\right)$ and structure $\mathcal{s}\left(\mathcal{I}, \bar{\mathcal{I}}\right)$. SSIM is expressed in Eq. (10-13):

$$SSIM\left(\mathcal{I}, \bar{\mathcal{I}}\right) = \ell\left(\mathcal{I}, \bar{\mathcal{I}}\right) c\left(\mathcal{I}, \bar{\mathcal{I}}\right) \mathcal{s}\left(\mathcal{I}, \bar{\mathcal{I}}\right) \tag{10}$$

$$\mathfrak{l} = \frac{2\eta_I \eta_{\bar{\jmath}} + c1}{\eta_I^2 + \eta_{\bar{\jmath}}^2 + c1} \tag{11}$$

$$\mathfrak{c} = \frac{2\sigma_I \sigma_{\bar{\jmath}} + c2}{\sigma_I^2 + \sigma_{\bar{\jmath}}^2 + c2} \tag{12}$$

$$\mathfrak{s} = \frac{\sigma_{\jmath\bar{\jmath}} + c3}{\sigma_I \sigma_{\bar{\jmath}} + c3} \tag{13}$$

where, η_I and $\eta_{\bar{\jmath}}$ represent the luminance of the respective images. If both images have same luminance i.e. $\eta_I = \eta_{\bar{\jmath}}$, the maximum value of $\mathfrak{l}$ is one. Similarly, if contrast of both images are same, the maximum value of c is also one. Whereas, the structural comparison i.e. $\mathfrak{s}$ measures the correlation coefficients between the host and watermarked images. Here, σ_I and $\sigma_{\bar{\jmath}}$ represent the standard deviation, and $\sigma_{\jmath\bar{\jmath}}$ represents the covariance factors of host and watermarked images.

3) NORMALIZED CORRELATION (NCC)

NCC measures the similarity between the original $\mathcal{W}_{i,\jmath}$ and extracted watermark $\overline{\mathcal{W}}_{i,\jmath}$ images and it is used to evaluate the robustness of the watermark against various image processing and geometric attacks. NCC is expressed in Eq. (14):

$$NCC\left(\mathcal{W}, \overline{\mathcal{W}}\right) = \frac{\sum_{i=1}^{m}\sum_{j=1}^{n}[\mathcal{W}_{i,j} - \lambda^{W}][\overline{\mathcal{W}}_{i,j} - \lambda^{\overline{\mathcal{W}}}]}{\sqrt{\sum_{i=1}^{m}\sum_{j=1}^{n}[W_{i,j} - \lambda^{W}]^2}\sqrt{\sum_{i=1}^{m}\sum_{j=1}^{n}[\overline{\mathcal{W}}_{i,j} - \lambda^{\overline{\mathcal{W}}}]^2}} \tag{14}$$

where, m and n represent the number of pixels in the watermark image, while λ^{W} and $\lambda^{\overline{\mathcal{W}}}$ represent the mean values of the original and extracted watermarks, respectively.

4) BIT ERROR RATE (BER)

Along with NCC, we have also used BER for robustness analysis between the original $\mathcal{W}_{i,\jmath}$ and extracted watermark $\overline{\mathcal{W}}_{i,\jmath}$ images. BER is expressed in Eq. (15):

$$BER\left(\mathcal{W}, \overline{\mathcal{W}}\right) = \frac{\sum_{i=1}^{m}\sum_{j=1}^{n}\mathcal{W}_{i,j} \otimes \overline{\mathcal{W}}_{i,j}}{m \times n} \tag{15}$$

where, $m \times n$ represent the dimensions of original and extracted watermark images.

C. PERCEPTUAL QUALITY ANALYSIS OF OUR PROPOSED WATERMARKING ALGORITHM

We have evaluated our proposed watermarking algorithm for perceptual changes and preservation of the patient health information in the form of EPR, associated with the medical images, for automated retinal diagnostics. Perceptual quality analysis is performed to check the efficiency of our proposed watermarking algorithm. In an efficient algorithm, the watermarked medical images must be highly imperceptible and visually identical to the original medical images to allow precise medical diagnosis by doctors. Figure 9(a) and 9(b) shows some of the randomly selected original OCT and fundus scans

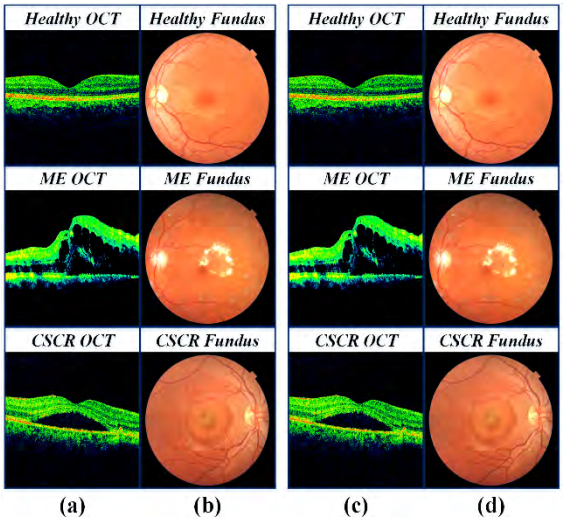

FIGURE 9. Randomly selected test scans. (a) Original retinal OCT scans. (b) Original retinal fundus scans. (c) Watermarked retinal OCT scans. (d) Watermarked retinal fundus scans.

for each retinal pathology, while Figure 9(c) and 9(d) shows their respective watermarked OCT and fundus scans, used as test scans in our study. PSNR and SSIM are calculated for original and watermarked retinal scans, to evaluate the perceptual transparency and imperceptibility of our proposed watermarking algorithm. The similarity between original and watermarked images is shown by high PSNR value and in terms of SSIM, the maximum value is one, which shows that the original and watermarked images are completely identical. In our proposed study, the deterioration in the retinal scans during the process of watermarking is measured using PSNR and SSIM metrics. Table 3 shows the values of PSNR and SSIM between original and watermarked retinal scans.

Similarly, NCC and BER are calculated to evaluate the robustness and loss less recovery of EPR for patient identification and integrity verification. NCC measures the similarity between two images, and therefore, it is used to measure the quality of the recovered watermark when compared with the original, in watermarking. The maximum value of NCC is one, which shows that the original and extracted watermark images are completely identical. Likewise, BER measures the bit error rate between the original and extracted watermark contents. Figure 10 shows some of the randomly selected watermark EPR images that are recovered from the watermarked retinal scans and Table 4 shows the values of NCC and BER between original and recovered EPR images.

In our proposed study, the watermarked retinal scans have mean value of PSNR over 60 dB and SSIM equal to one, which shows that the proposed watermarking algorithm is highly imperceptible and does not deteriorate the visual quality of retinal scans even after watermark embedding. Similarly, the recovered EPR images have mean value of NCC equal to one and zero BER, which shows that the proposed watermarking algorithm is highly robust and achieves

TABLE 3. PSNR and SSIM between original and watermarked retinal scans.

Type	Test Scans	PSNR	SSIM
Healthy	OCT 1	64.4255	1
	OCT 2	63.2848	1
	OCT 3	63.5368	1
	OCT 4	67.5717	1
	OCT 5	66.1825	1
	OCT 6	63.5388	1
	OCT 7	64.4333	1
	OCT 8	65.7600	1
	OCT 9	64.9955	1
ME	OCT 10	66.2968	1
	OCT 11	63.9028	1
	OCT 12	66.5468	1
	OCT 13	63.2140	1
	OCT 14	65.4560	1
	OCT 15	67.0126	1
CSCR	OCT 16	63.7580	1
	OCT 17	65.1415	1
	OCT 18	67.5834	1
	OCT 19	66.9727	1
	OCT 20	67.7997	1
	OCT 21	66.2981	1
Healthy	Fundus 1	63.2331	1
	Fundus 2	67.2541	1
	Fundus 3	66.4118	1
ME	Fundus 4	66.8023	1
	Fundus 5	66.7301	1
	Fundus 6	64.9955	1
Mean (Total Dataset)	OCT	64.8726	1
	Fundus	65.0162	1

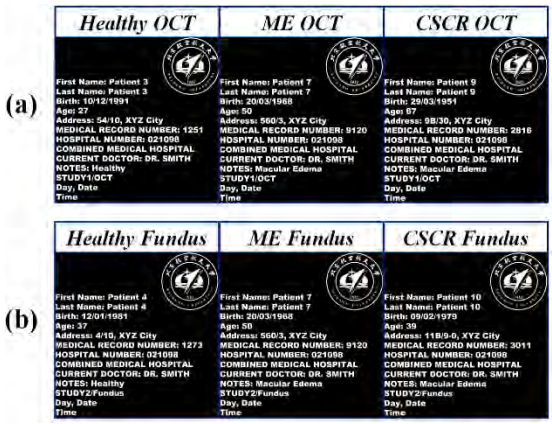

FIGURE 10. Randomly selected EPR images. (a) Recovered EPR from watermarked retinal OCT scans. (b) Recovered EPR from watermarked retinal fundus scans.

loss less recovery of patient health information in the form of EPR.

D. ROBUSTNESS OF OUR PROPOSED WATERMARKING ALGORITHM AGAINST COMMON IMAGE PROCESSING OPERATIONS

It is evident that computer-aided diagnostic systems usually involve different image processing stages to facilitate automated detection of diseases. Therefore, before undergoing automated retinal diagnostics, the watermarked retinal scans are tested against various common image processing operations to verify that the integrity of the embedded EPR, as watermark remains unaffected in the process. We performed various image processing operations such as Histogram Equalization (HE), Contrast Enhancement (CE), scaling, rotation, median filtering, sharpening, salt and pepper noise, Gaussian noise, cropping etc. on the watermarked retinal scans. Figure 11 shows these different operations against a test watermarked OCT scan along with the recovered EPR watermarks. The relevant values of PSNR and SSIM for watermarked OCT scan and values of NCC and BER for the recovered EPR image, after applying each image processing operation are listed in Table 5.

In addition, we have also evaluated the robustness of our proposed watermarking scheme against Stirmark 4.0, which is a watermarking benchmark consisting of a number of image processing and geometric attacks [36]. The results from Table 6 validate that our proposed watermarking system is highly robust against various image processing and geometric attacks.

TABLE 4. NCC and BER between original and recovered EPR.

Type	Test Scans	NCC	BER
Healthy	OCT 1	1	0
	OCT 2	1	0
	OCT 3	1	0
	OCT 4	1	0
	OCT 5	1	0
	OCT 6	1	0
	OCT 7	1	0
	OCT 8	1	0
	OCT 9	1	0
ME	OCT 10	1	0
	OCT 11	1	0
	OCT 12	1	0
	OCT 13	1	0
	OCT 14	1	0
	OCT 15	1	0
CSCR	OCT 16	1	0
	OCT 17	1	0
	OCT 18	1	0
	OCT 19	1	0
	OCT 20	1	0
	OCT 21	1	0
Healthy	Fundus 1	1	0
	Fundus 2	1	0
	Fundus 3	1	0
ME	Fundus 4	1	0
	Fundus 5	1	0
	Fundus 6	1	0
Mean (Total Dataset)	OCT	1	0
	Fundus	1	0

E. UNCOMPROMISED AUTOMATED RETINAL DIAGNOSTICS

Since, it is an important design requirement of medical image watermarking that embedding watermark contents should not distort the medical images, and should retain all the

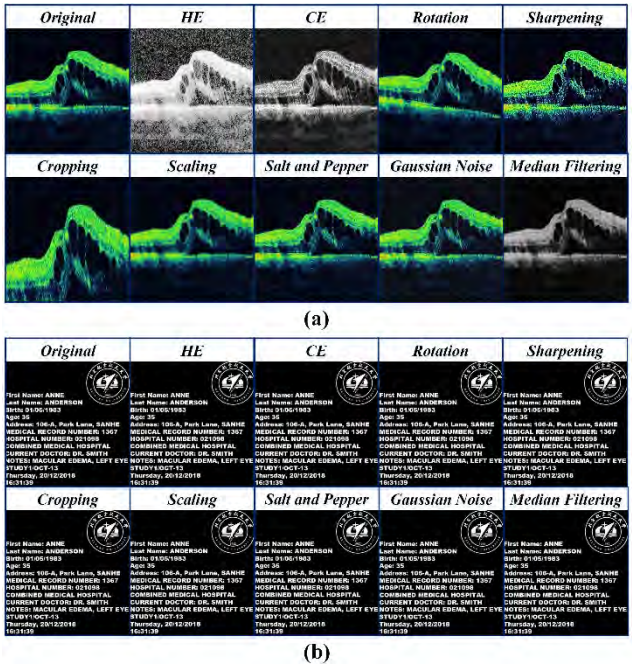

FIGURE 11. Extraction of EPR under various image processing operations. (a) Test watermarked OCT scan under each image processing operation. (b) Recovered EPR against each image processing operation.

TABLE 5. Robustness against various image processing operations.

Image Processing Operation	Watermarked Scan		Recovered EPR	
	PSNR	SSIM	NCC	BER
Histogram Equalization	9.6474	0.3599	1.0000	0.0000
Scaling (reduced 1/25)	25.2040	0.8981	1.0000	0.0000
Rotation (5 degrees clockwise)	30.4549	0.9719	1.0000	0.0000
Contrast Enhancement (contrast enhancement limit= 0.01)	25.6788	0.7175	1.0000	0.0000
Median Filtering (4 × 4)	41.4479	0.9816	1.0000	0.0000
Sharpening (standard deviation= 2, strength factor= 2)	34.7350	0.9913	1.0000	0.0000
Salt & Pepper Noise (noise density = 0.01)	24.2008	0.8232	1.0000	0.0000
Gaussian Noise (mean= 0, variance= 0.01)	21.0506	0.6269	1.0000	0.0000
Cropping (more than 25%)	16.0503	0.7775	1.0000	0.0000

important information for accurate medical diagnosis. Therefore, to study the influence of EPR embedding on the retinal scans, during the process of automated computer-aided diagnosis of retinal diseases, several experiments were performed. We used our existing machine learning algorithms for automated retinal diagnostics to test the imperceptibility of the proposed watermarking algorithm, and most importantly to observe if all the significant clinical features of the retinal scans remain preserved after watermarking process leading to accurate detection of retinal abnormalities.

We examined original and watermarked retinal scans to diagnose two common retinal diseases such as ME and CSCR. In addition, we have performed a comparative analysis in terms of features extraction, objects segmentation and detection of abnormalities of retina, to study if embedding the EPR contents in the retinal scans have affected them for medical diagnosis. Figure 12 shows the comparison between original and watermarked retinal scans for the following four stages of automated retinal diagnostic system: (i) Input scan, (ii) Preprocessing, (iii) Structure Tensors (ST) and (iv) Classification. The input scan shows the original retinal scan without any processing. Since, the original retinal scan contains speckle noises and other artifacts that may affect the diagnosis of abnormalities. Therefore, the preprocessing stage is an important stage for any computer-aided diagnostic system in order to remove such artifacts and denoise the input scan. In our existing algorithms, we have performed various image enhancement operations during the preprocessing stage such as Gaussian filtering in [32], Wiener filtering in [29]–[33], blob filtering in [30], image resizing in [29]–[33], contrast adjustments in [29]–[33], histogram equalization in [31], morphological operations in [29], [30], [33] to prepare the input scan for further processing. Next, to extract distinguished features between different retinal pathologies, we used 2D structure tensors approach. Structure tensors is also known as Forstner operator, computes image gradients by using Gaussian derivatives. It is useful for low-level feature analysis such as detecting edges and boundaries [37], [38]. The ST stage in Figure 12 shows the most coherent tensor in each algorithm. The input retinal scan is classified in the last stage based on the features extracted by using ST approach and the training dataset of machine learning classifiers such as Support Vector Machine (SVM) in [29], Discriminant Analysis (DA) in [30], [33], K-Nearest Neighbors (K-NN) in [31]. It can be easily observed from Figure 12 that the original and watermarked retinal scans at all the stages are completely identical and indicate no visible difference, which shows that the proposed watermarking algorithm is highly imperceptible and does not affect the process of automated retinal diagnostic system.

As mentioned earlier, we have evaluated original and watermarked retinal scans against our existing algorithms [29]–[33]. We estimated different features to classify retinal diseases using both OCT and fundus scans. In case of OCT scans, these features are based on separation between NLF and RPE retinal layers, presence of cystic fluid between these layers and the geometry of cystic fluid. While, in case of fundus scans, these features are based on presence of hard exudates in the macula region. Table 7 shows the comparison of these features (F1, F2, F3, F4, F5) extracted from original and watermarked retinal scans. It can be seen that minor difference is observed in these feature values for each existing algorithm. Table 8 shows the details of our existing algorithms.

TABLE 6. Evaluation of robustness against benchmark Stirmark 4.0.

Attack	Parameter	NCC between Original and Recovered EPR (Watermark)					
		OCT Scan 1	OCT Scan 2	Mean* (OCT)	Fundus Scan 1	Fundus Scan 2	Mean* (Fundus)
No Attack	-	1.0000	1.0000	1.0000	1.0000	1.0000	1.0000
JPEG Compression	50	0.9995	0.9994	0.9996	0.9992	0.9989	0.9991
	70	0.9998	0.9997	0.9998	0.9998	0.9998	0.9998
	90	1.0000	1.0000	1.0000	1.0000	1.0000	0.9999
Median Filtering	3 × 3	1.0000	1.0000	1.0000	1.0000	1.0000	1.0000
	5 × 5	0.9998	0.9998	0.9999	0.9997	0.9999	0.9999
Random Bending	-	0.9517	0.9578	0.9532	0.9571	0.9527	0.9534
Shearing	(x, y) = (0%, 5%)	0.9601	0.9642	0.9635	0.9638	0.9617	0.9621
	(x, y) = (5%, 0%)	0.9674	0.9681	0.9675	0.9691	0.9631	0.9658
	(x, y) = (1%, 1%)	0.9821	0.9857	0.9836	0.9871	0.9861	0.9854
Centered Crop	5%	0.9841	0.9871	0.9869	0.9845	0.9863	0.9858
Rotation	2° + Crop[a]	0.9896	0.9874	0.9886	0.9845	0.9867	0.9871
	5° + Crop[a]	0.9791	0.9788	0.9790	0.9762	0.9801	0.9791
	10° + Crop[a]	0.9761	0.9741	0.9763	0.9754	0.9766	0.9768
	15° + Crop[a]	0.9738	0.9729	0.9736	0.9748	0.9719	0.9725
	2° + Scaling[b]	0.9971	0.9952	0.9969	0.9941	0.9982	0.9971
	5° + Scaling[b]	0.9871	0.9853	0.9870	0.9863	0.9881	0.9874
	10° + Scaling[b]	0.9851	0.9831	0.9837	0.9829	0.9841	0.9827
	2° + Crop[a] + Scaling[b]	0.9684	0.9647	0.9651	0.9663	0.9678	0.9653
	5° + Crop[a] + Scaling[b]	0.9632	0.9631	0.9634	0.9631	0.9629	0.9638
	10° + Crop[a] + Scaling[b]	0.9597	0.9608	0.9601	0.9617	0.9604	0.9599
Scaling	0.75 ×	0.9851	0.9843	09847	0.9861	0.9843	0.9850
	0.90 ×	0.9991	0.9989	0.9991	0.9987	0.9988	0.9989
	1.1 ×	0.9997	0.9997	0.9997	0.9998	0.9997	0.9997
	1.5 ×	0.9995	0.9993	0.9994	0.9994	0.9993	0.9994
Random Distortion	0.95	0.9947	0.9941	0.9944	0.9951	0.9948	0.9943
Flip	Horizontal	1.0000	1.0000	1.0000	1.0000	1.0000	1.0000
	Vertical	1.0000	1.0000	1.0000	1.0000	1.0000	1.0000
Linear Geometric Transform	1.008	0.9778	0.9769	0.9774	0.9768	0.9748	0.9765
	1.012	0.9698	0.9682	0.9681	0.9692	0.9679	0.9686

*Mean value is computed for complete OCT and fundus datasets, [a]5% centered crop, [b]1.5 × scaling.

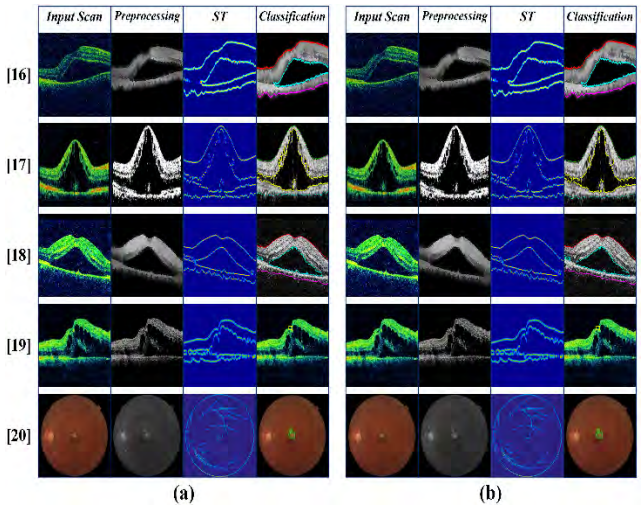

FIGURE 12. Comparative analysis using original and watermarked scans based on our existing algorithms for automated retinal diagnostics. (a) Original retinal scans at various stages of automated retinal diagnostics system. (b) Watermarked retinal scans at various stages of automated retinal diagnostics system.

Experimental results shown in Table 9 indicate that we achieved same accuracy with watermarked retinal scans as with original retinal scans for each existing algorithm. Additionally, mean NCC value of each extracted feature is calculated as shown in Table 9, which are found to be slightly less than one in each case as observed.

Figure 13(a) and 13(b) shows the comparative analysis between some of the randomly selected OCT test scans; displaying healthy eye, ME and CSCR affected eyes, and fovea localization, respectively. We loaded unlabeled watermarked OCT scans into the proposed framework to evaluate them against the automated retinal diagnostics algorithms and subsequently achieved the same diagnosis results with watermarked OCT scans as with original OCT scans for each existing algorithm as shown. These results indicate that the proposed framework correctly classified the watermarked OCT scans and without affecting the embedded watermark contents, it achieved loss less recovery of EPR in each case. Similarly, Figure 13(c) and 13(d) shows the comparative analysis of automated retinal diagnostic algorithms when applied to some of the randomly selected fundus test scans; displaying healthy eye, ME affected eye, blood vessel segmentation and hard exudates extraction from the input fundus scan, respectively. These results also indicate that the proposed framework produced same diagnosis results with watermarked fundus scans as with original fundus scans in each case without affecting the patient health information embedded in these scans.

TABLE 7. Comparison of Extracted Features between original and watermarked retinal scans.

Ref.	Subjects	Existing (Without Watermarked Scans)					Proposed (With Watermarked Scans)					Diagnosed Pathology
		F1	F2	F3	F4	F5	F1	F2	F3	F4	F5	
[29]	OCT 1	34.13	19.58	14.55	0	0	34.44	19.51	15.39	0	0	Healthy
	OCT 2	38.36	18.26	20.11	174.34	983.24	38.07	18.18	19.75	174.25	1002.85	
	OCT 3	39.69	23.02	16.67	140.28	1328.8	40.17	23.11	16.10	140.19	1293.83	
	Mean	40.01	21.94	18.07	117.43	1087.2	40.28	21.86	19.05	117.33	1060.08	
	OCT 1	72.23	36.25	35.98	7023.88	56835	71.42	36.17	35.41	7006.99	56867	ME
	OCT 2	65.62	39.42	26.19	3201.17	25871	64.63	39.50	25.83	3187.40	25850	
	OCT 3	48.42	25.66	22.75	18400.9	32093	48.50	25.58	22.11	18436.0	32108	
	Mean	54.64	39.17	24.28	15194.3	28148	54.08	39.22	24.67	15162.3	28122	
	OCT 1	63.5	43.39	20.11	8724.1	12940	63.37	43.30	19.34	8743.2	12963	CSCR
	OCT 2	71.7	35.98	35.72	26443.2	13051	72.51	36.08	35.28	26468.8	13015	
	OCT 3	64.29	38.1	26.19	11827.1	10417	63.30	38.17	26.71	11790.5	10381	
	Mean	59.74	32.03	27.71	13430.4	12416	59.63	31.93	28.42	13400.5	12448	
[30]	OCT 1	37.83	01.72	36.11	-	-	36.89	1.65	35.14	-	-	Healthy
	OCT 2	39.16	0.87	38.29	-	-	39.23	0.78	37.93	-	-	
	OCT 3	42.74	03.96	38.78	-	-	42.04	4.03	37.93	-	-	
	Mean	41.19	03.07	39.67	-	-	40.40	3.00	40.42	-	-	
	OCT 1	61.27	04.92	56.35	-	-	61.83	4.86	55.39	-	-	ME
	OCT 2	79.41	06.11	73.3	-	-	78.52	6.17	73.22	-	-	
	OCT 3	113.20	07.50	105.7	-	-	112.30	7.43	105.31	-	-	
	Mean	86.47	06.13	80.34	-	-	85.83	6.04	81.02	-	-	
[31]	OCT 1	136.9119	0	136.9119	-	-	136.7309	0	136.5945	-	-	Healthy
	OCT 2	127.1814	0	127.1814	-	-	126.9245	0	127.4503	-	-	
	OCT 3	115.9334	0	115.9334	-	-	115.7104	0	115.2078	-	-	
	Mean	132.5173	0.0751	132.5924	-	-	132.4276	0.0729	131.9491	-	-	
	OCT 1	199.1720	30.9241	230.0961	-	-	199.3236	30.8280	229.4850	-	-	CSCR
	OCT 2	249.4307	49.5096	249.9404	-	-	248.7951	49.5981	250.6178	-	-	
	OCT 3	219.8254	61.3842	281.2096	-	-	218.8827	61.3321	281.1144	-	-	
	Mean	204.8513	52.4856	257.3369	-	-	204.4646	52.4167	257.7182	-	-	
[33]	Fundus 1	-	-	-	-	0	-	-	-	-	0	Healthy
	Fundus 2	-	-	-	-	11.57	-	-	-	-	11.29	
	Fundus 3	-	-	-	-	0	-	-	-	-	0	
	Mean	-	-	-	-	5.08	-	-	-	-	4.22	
	Fundus 1	-	-	-	-	47.25	-	-	-	-	46.93	ME
	Fundus 2	-	-	-	-	53.19	-	-	-	-	53.93	
	Fundus 3	-	-	-	-	80.91	-	-	-	-	80.73	
	Mean	-	-	-	-	57.28	-	-	-	-	58.12	

TABLE 8. Existing algorithms details.

Algorithm	Dataset Used	Imaging Modality	Total scans	Retinal Pathology
[29]	BIOMISA	OCT	90	Healthy, ME, CSCR
[30]	DUKE	OCT	30	Healthy, ME
[31]	BIOMISA	OCT	80	Healthy, CSCR
[32]	BIOMISA	OCT	120	Healthy, ME, CSCR
[33]	BIOMISA	OCT/ Fundus	71/ 71	Healthy, ME

F. COMPARISON WITH EXISTING WATERMARKING TECHNIQUES

We have also drawn a comparison of our proposed watermarking framework with some of the existing studies related to medical image watermarking. The state of art comparison in terms of perceptual quality analysis and influence of embedding watermark on the automated diagnostic results is shown in Table 10. It can be observed that the proposed watermarking framework achieved value of PSNR over 60 dB and SSIM equal to one, which is more than the reported results in the existing studies. In addition, it achieved value of NCC equal to one and zero BER with presenting no significant changes on the automated diagnostic results associated with the retinal scans. It is apparent from Table 10 that various watermarking techniques have been presented in the past but none observed the influence of watermark embedding on the diagnosis results associated with the medical images. Hence, the proposed imperceptible watermarking framework can be considered to address the security issues associated with medical images and aiding uncompromised computer-aided medical analysis for eHealth applications.

IV. DISCUSSION

Based on the extensive analysis, the merits of our proposed watermarking framework can be concluded as following. First, mean value of PSNR over 60 dB and SSIM equal to one between original and watermarked retinal scans as listed in Table 3 indicates that the proposed watermarking framework is highly imperceptible in nature, and does not distort the retinal scans during the process of watermarking. Second, the proposed watermarking algorithm is highly

TABLE 9. Comparison of results achieved between original and watermarked retinal scans.

Ref.	*Type*	Existing (Without Watermarked Scans)				Proposed (With Watermarked Scans)				NCC (mean all dataset)				
		CC	*Sensitivity*	*Specificity*	*Accuracy*	*CC*	*Sensitivity*	*Specificity*	*Accuracy*	*F1*	*F2*	*F3*	*F4*	*F5*
[29]	A	28 / 30	100 %	93.33 %	**97.77 %**	28 / 30	100 %	93.33 %	**97.77 %**	0.993	0.996	0.946	0.999	0.975
	B	30 / 30				30 / 30				0.990	0.999	0.984	0.998	0.999
	C	30 / 30				30 / 30				0.998	0.997	0.974	0.998	0.997
[30]	A	13 / 15	100 %	86.66 %	**93.33 %**	13 / 15	100 %	86.66 %	**93.33 %**	0.981	0.977	0.981	-	-
	B	15 / 15				15 / 15				0.993	0.985	0.992	-	-
[31]	A	40 / 40	100 %	100 %	**100 %**	40 / 40	100 %	100 %	**100 %**	0.999	0.971	0.995	-	-
	C	40 / 40				40 / 40				0.998	0.999	0.999	-	-
[33]*	A	42 / 45	100 %	93.33 %	**95 %**	42 / 45	100 %	93.33 %	**95 %**	-	-	-	-	1
	B	15 / 15				15 / 15				-	-	-	-	0.985

*Results in [33] are shown in terms of number of patients and not number of scans; CC= Correctly Classified cases, A= Healthy, B= Macular Edema (ME), C= Central Serous Chorioretinopathy (CSCR).

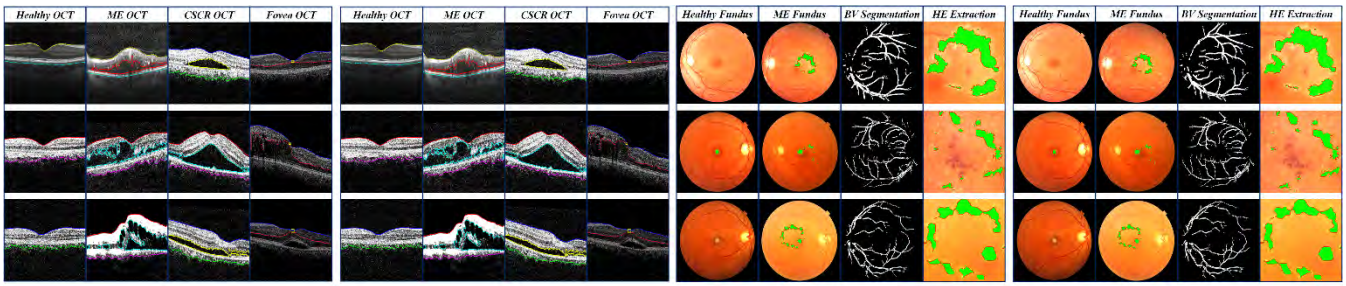

FIGURE 13. Comparative analysis of automated retinal diagnostics using original and watermarked scans based on our existing algorithms. (a) Diagnosis results with original OCT scans. (b) Diagnosis results with watermarked OCT scans. (c) Diagnosis results with original fundus scans. (d) Diagnosis results with watermarked fundus scans.

robust against various image processing operations as shown in Figure 11 and Table 6, which are commonly used in any automated diagnostic system for medical analysis. Furthermore, it is observed that there is a tradeoff between robustness (NCC), imperceptibility (PSNR) and capacity. Where, if we improve the robustness of the watermarking technique, the capacity in return increases and imperceptibility decreases. In our proposed study, we tried to balance the tradeoff between automated retinal diagnosis and loss less recovery of EPR. Since, various image processing operations during the automated retinal diagnosis stage do not deteriorate the quality of the watermarked scan severely and maintain a healthy PSNR, therefore, our main challenge was to achieve the loss less recovery of EPR as watermark image in order to perform the functionalities of medical image authentication and accurate patient identification.

Third, we evaluated our existing algorithms based on automated retinal diagnostics [29]–[33] by embedding EPR as a watermark in the original retinal scans. The proposed watermarking technique did not affect the results of automated diagnostics and we achieved the same sensitivity, specificity and accuracy results as with non-watermarked retinal scans as shown in Table 7 and Table 11. However, by embedding the EPR as watermark, we have preserved the patient information, which is used for authentication purpose and accurate patient identification to prevent errors in medical diagnosis. Hence, the proposed framework is suitable to secure medical data dissemination over the open channel and protect patient health information from theft or modification.

Fourth, mean value of NCC equal to one and zero BER between original and recovered EPR as listed in Table 4 indicates that the proposed watermarking framework achieved accurate and loss less recovery of patient health information from the watermarked retinal scans for authentication purposes. Loss less recovery of watermark (EPR) in our proposed scheme is mainly due to two reasons: (i) the extraction process is irrespective of the predicted classes (true positive, true negative, false positive, false negative), and (ii) the proposed hybrid watermarking scheme is based on two transforms. Curvelet transform allows the watermark bits to be embedded or casted onto more significant positions and directions in the subbands of the image, and SVD transform makes the scheme highly resistant to most of the image processing and geometric attacks. Where, although the singular values might be mostly affected, still it substantially preserves the overall integrity of the data. Fifth, the size of the watermark image can be applied flexibly and is not limited to 512×512 as used in this proposed study. Finally, the comparison with existing watermarking techniques as shown in Table 10 indicates that the proposed watermarking framework outdid them with relatively good performance. Hence, the proposed imperceptible watermarking framework can be considered as a significant contribution to address the issues of medical image security and authentication in computer vision based automated diagnosis of medical disorders in an eHealth arrangement.

TABLE 10. Comparison with state-of-the-art existing watermarking techniques.

Ref.	Description	Dataset Details	Methodology/ Watermarking Technique	Perceptual Quality Analysis				Influence of Embedding Watermark on Automated Diagnostic Results
				PSNR[1] (dB)	Correlation[1]	NCC[2]	BER[2]	
[39]	Privacy of patient data	X-Ray, CT Scan and MRI images	Watermarking based on DWT and DCT	40 to 45	Correlation is approx. 1	-	-	-
[40]	Security of medical image databases	CT Scan images	Reversible watermarking based on LSB	31.6209	-	-	-	-
[41]	Watermark compression in medical images	Ultrasound images	Watermarking using LZW compression technique	51.5351	-	-	-	-
[42]	Detect tampering of medical images	CT Scan, MRI, Ultrasound and PET Scan images	Watermarking based on IWT	49.41	MSSIM=0.9776	1	-	-
[43]	Protecting medical images against noise	MRI images	Spatial domain watermarking	41.73	SSIM=0.9127	-	0.96	-
[44]	Information hiding in medical images	CT Scan images	Watermarking based on DCT	41.1521	SSIM=0.9857	0.9923	0.68	-
[45]	Security of medical information	MRI, CT Scan and Ultrasound images	Watermarking based on DWT and DCT	37.0424	-	1	0	-
[46]	Blind medical image watermarking	X-Ray, CT Scan and Mammography images	Watermarking based on DWT and SVD	45.4666	SSIM=0.9736	0.99	0.0039	-
[47]	Hybrid watermarking for security of medical images	OCT Scans and Fundus images	Watermarking based on FCT and RPCA	51.9537	SSIM=0.9981	0.9985	0.2772	-
PF	**Imperceptible watermarking framework for securing medical images in automated diagnosis of retinal pathologies**	**OCT Scans and Fundus images**	**Watermarking using Curvelet domain and SVD**	**65**	**SSIM=1**	**1**	**0**	**No significant changes are observed on the automated diagnostic results due to EPR embedding**

[1]Values between Original and Watermarked Image, [2]Values between Original and Recovered Watermark; MRI= Magnetic Resonance Imaging, CT= Computerized Tomography, PET= Positron Emission Tomography, DWT= Discrete Wavelet Transform, DCT= Discrete Cosine Transform, LSB= Least Significant Bit, LZW= Lempel–Ziv–Welch, IWT= Integer Wavelet Transform, RPCA= Robust Principle Component Analysis, PF= Proposed Framework, MSSIM= Mean Structure Similarity Index, dB= Decibel.

V. CONCLUSION AND FUTURE WORK

With the ever-growing age of technology, the digitally driven eHealth services are seen to be very promising. However, due to an increase in crimes related to medical data theft, stealing or altering patient health information, the security and verification of medical records have become a great challenge in the electronic healthcare environment. Identification of medical images for automated computer-aided diagnosis is considered an essential requirement for eHealth applications. This paper is an effort towards developing an imperceptible watermarking framework to solve the issues of authentication of retinal scans and verification of patient health information for automated retinal diagnostics in an eHealth Arrangement. In this proposed study, EPR is embedded in the retinal scans with maintaining the overall perceptual transparency and integrity of the medical data. The proposed framework achieves uncompromised automated diagnosis of retinal pathologies and loss less recovery of patient health information for authentication purposes. Experiment results indicate that the proposed watermarking algorithm is highly imperceptible and robust, and ensures no influence of EPR embedding on the automated retinal diagnosis results. In the future, this work can be extended to optimize the performance with respect to other mediums of multimedia such as 3-Dimensional (3-D) volumetric eye scans, and to other imaging modalities such as MRI scans, Chest X-Rays (CXRs) etc. for automated diagnosis of different medical disorders.

ACKNOWLEDGMENT

The authors would like to thank Vision and Image Processing (VIP) Laboratory, Duke University and BioMedical Image and Signal Analysis (BIOMISA) Laboratory for sponsoring the highly detailed and annotated datasets. *(Bilal Hassan and Ramsha Ahmed contributed equally to this work.)*

REFERENCES

[1] C. S. Kruse, B. Smith, H. Vanderlinden, and A. Nealand, "Security techniques for the electronic health records," *J. Med. Syst.*, vol. 41, no. 8, pp. 127–135, Jul. 2017.
[2] F. F. Ozair, N. Jamshed, A. Sharma, and P. Aggarwal, "Ethical issues in electronic health records: A general overview," *Perspect. Clin. Res.*, vol. 6, no. 2, pp. 73–76, 2015.
[3] Y. Tan, J. Qin, L. Tan, H. Tang, and X. Xiang, "A survey on the new development of medical image security algorithms," in *Proc. Int. Conf. Cloud Comput. Secur. (ICCCS)*, 2018, pp. 458–467.
[4] W. Sun, Z. Cai, Y. Li, F. Liu, S. Fang, and G. Wang, "Security and privacy in the medical Internet of Things: A review," *Secur. Commun. Netw.*, vol. 2018, Jan. 2018, Art. no. 5978636.
[5] A. G. Bors and M. Luo, "Optimized 3D watermarking for minimal surface distortion," *IEEE Trans. Image Process.*, vol. 22, no. 5, pp. 1822–1835, May 2013.
[6] Z. Li and A. G. Bors, "Selection of robust and relevant features for 3-D steganalysis," *IEEE Trans. Cybern.*, to be published.
[7] J.-S. Coron, "What is cryptography?" *IEEE Security Privacy*, vol. 4, no. 1, pp. 70–73, Jan. 2006.
[8] G. Mehta, M. K. Dutta, and P. S. Kim, "An efficient and lossless cryptosystem for security in tele-ophthalmology applications using chaotic theory," in *Proc. Ophthalmology, Breakthroughs Res. Pract.*, 2018, pp. 189–210.
[9] S. Katzenbeisser and F. A. P. Petitcolas, *Digital Watermarking*. London, U.K.: Artech House, 2000.
[10] R. Ahmed, M. M. Riaz, and A. Ghafoor, "Attack resistant watermarking technique based on fast curvelet transform and robust principal component analysis," *Multimedia Tools Appl.*, vol. 77, no. 8, pp. 9443–9453, Apr. 2018.
[11] T. D. Pham, D. Tran, and W. Ma, "Ownership protection of outsourced biomedical time series data based on optimal watermarking scheme in data mining," *Australas. J. Inf. Syst.*, vol. 21, Nov. 2017. doi: 10.3127/ajis.v21i0.1541.
[12] E. Elbasi and V. Kaya, "Robust medical image watermarking using frequency domain and least significant bits algorithms," in *Proc. Int. Conf. Comput. Sci. Eng. (ICCSE)*, Kuwait City, Kuwait, Mar. 2018, pp. 1–5.
[13] A. U. Rahman, K. Sultan, D. Musleh, N. Aldhafferi, A. Alqahtani, and M. Mahmud, "Robust and fragile medical image watermarking: A joint venture of coding and chaos theories," *J. Healthcare Eng.*, vol. 2018, Apr. 2018, Art. no. 8137436.
[14] X. Han, C. Xiong, Y. Li, F. He, and H. Du, "RETRACTED ARTICLE: Medical image encryption technique in big media environment," in *Multimedia Tools and Applications*. New York, NY, USA: Springer, 2018, pp. 1–9.
[15] A. Al-Haj, A. Mohammad, and A. Amer, "Crypto-Watermarking of transmitted medical images," *J. Digit. Imag.*, vol. 30, no. 1, pp. 26–38, Feb. 2017.
[16] A. G. Bors and I. Pitas, "Image watermarking using DCT domain constraints," in *Proc. 3rd IEEE Int. Conf. Image Process.*, Lausanne, Switzerland, vol. 3, Sep. 1996, pp. 231–234.
[17] S. D. Lin and C.-F. Chen, "A robust DCT-based watermarking for copyright protection," *IEEE Trans. Consum. Electron.*, vol. 46, no. 3, pp. 415–421, Aug. 2000.
[18] C.-C. Lai and C.-C. Tsai, "Digital image watermarking using discrete wavelet transform and singular value decomposition," *IEEE Trans. Instrum. Meas.*, vol. 59, no. 11, pp. 3060–3063, Nov. 2010.
[19] S. Lagzian, M. Soryani, and M. Fathy, "A new robust watermarking scheme based on RDWT-SVD," *Int. J. Intell. Inf. Process.*, vol. 2, no. 1, pp. 22–29, Mar. 2011.
[20] P. Premaratne and C. C. Ko, "A novel watermark embedding and detection scheme for images in DFT domain," in *Proc. 7th Int. Conf. Image Process. Appl.*, Jul. 1999, pp. 780–783.
[21] S. Rastegar, F. Namazi, K. Yaghmaie, and A. Aliabadian, "Hybrid watermarking algorithm based on singular value decomposition and radon transform," *AEU-Int. J. Electron. Commun.*, vol. 65, no. 7, pp. 658–663, Jul. 2011.
[22] T. D. Hien, K. Miyara, I. Kei, F. F. Ali, Y. W. Chen, and Z. Nakao, "Digital watermarking based on curvelet transform," in *Proc. 9th Int. Symp. Signal Process. Appl.*, Sharjah, United Arab Emirates, Feb. 2007, pp. 1–4.
[23] E. J. Candès and D. L. Donoho, "New tight frames of curvelets and optimal representations of objects with piecewise C_2 singularities," *Commun. Pure Appl. Math.*, vol. 57, no. 2, pp. 219–266, Feb. 2004.
[24] D. L. Donoho and M. R. Duncan, "Digital curvelet transform: Strategy, implementation, and experiments," *Proc. SPIE*, vol. 4056, pp. 12–31, Apr. 2000.
[25] N. M. Makbol, B. E. Khoo, and T. H. Rassem, "Security analyses of false positive problem for the SVD-based hybrid digital image watermarking techniques in the wavelet transform domain," *Multimedia Tools Appl.*, vol. 77, no. 20, pp. 26845–26879, Oct. 2018.
[26] J. M. Guo and H. Prasetyo, "False-positive-free SVD-based image watermarking," *J. Vis. Commun. Image Represent.*, vol. 25, pp. 1149–1163, Jul. 2014.
[27] E. A. Swanson, J. A. Izatt, M. R. Hee, D. Huang, C. P. Lin, J. S. Schuman, C. A. Puliafito, and J. G. Fujimoto, "*In vivo* retinal imaging by optical coherence tomography," *Opt. Lett.*, vol. 18, no. 21, pp. 1864–1866, 1993.
[28] S. Schmitz-Valckenberg, F. G. Holz, A. C. Bird, and R. F. Spaide, "Fundus autofluorescence imaging: Review and perspectives," *Retina*, vol. 28, no. 3, pp. 385–409, Mar. 2008.
[29] B. Hassan, G. Raja, T. Hassan, and M. U. Akram, "Structure tensor based automated detection of macular edema and central serous retinopathy using optical coherence tomography images," *J. Opt. Soc. Amer. A, Opt. Image Sci.*, vol. 33, no. 4, pp. 455–463, 2016.
[30] B. Hassan and G. Raja, "Fully automated assessment of macular edema using optical coherence tomography (OCT) images," in *Proc. Int. Conf. Intell. Syst. Eng. (ICISE)*, pp. 5–9, Jan. 2016.
[31] B. Hassan, R. Ahmed, and B. Li, "Computer aided diagnosis of idiopathic central serous chorioretinopathy," in *Proc. 2nd IEEE Adv. Inf. Manage., Communicates, Electron. Automat. Control Conf. (IMCEC)*, May 2018, pp. 824–828.
[32] B. Hassan, R. Ahmed, and B. Li, "Automated foveal detection in OCT scans," in *Proc. IEEE Int. Symp. Signal Process. Inf. Technol. (ISSPIT)*, Dec. 2018, pp. 419–422.
[33] B. Hassan, R. Ahmed, B. Li, O. Hassan, and T. Hassan, "Automated retinal edema detection from fundus and optical coherence tomography scans," in *Proc. 5th Int. Conf. Control, Automat. Robot. (ICCAR)*, Beijing, China, Apr. 2019, pp. 1–6.
[34] T. Hassan, M. U. Akram, M. F. Masood, and U. Yasin, "BIOMISA retinal image database for macular and ocular syndromes," in *Proc. Int. Conf. Image Anal. Recognit.*, 2018, pp. 695–705.
[35] P. P. Srinivasan, L. A. Kim, P. S. Mettu, S. W. Cousins, G. M. Comer, J. A. Izatt, and S. Farsiu, "Fully automated detection of diabetic macular edema and dry age-related macular degeneration from optical coherence tomography images," *Biomed. Opt. Express*, vol. 5, no. 10, pp. 3568–3577, Sep. 2014.
[36] F. A. P. Petitcolas, R. J. Anderson, and M. G. Kuhn, "Attacks on copyright marking systems," in *Proc. Int. Workshop Inf. Hiding*, 1998, pp. 218–238.
[37] U. Köthe, "Edge and junction detection with an improved structure tensor," in *Proc. Joint Pattern Recognit. Symp.* Berlin, Germany: Springer, 2003, pp. 25–32.
[38] T. Brox, R. Van Den Boomgaard, F. Lauze, J. Van De Weijer, J. Weickert, P. Mrázek, and P. Kornprobst, "Adaptive structure tensors and their applications," in *Visualization and Processing of Tensor Fields*. Berlin, Germany: Springer, 2006, pp. 17–47.
[39] A. Mehto and N. Mehra, "Adaptive lossless medical image watermarking algorithm based on DCT & DWT," *Procedia Comput. Sci.*, vol. 78, pp. 88–94, Jan. 2016.
[40] F. Abbasi and N. A. Memon, "Reversible watermarking for the security of medical image databases," in *Proc. 21st Saudi Comput. Soc. Nat. Comput. Conf. (NCC)*, 2018, pp. 1–6.
[41] G. Badshah, S.-C. Liew, J. M. Zain, and M. Ali, "Watermark compression in medical image watermarking using Lempel-Ziv-welch (LZW) lossless compression technique," *J. Digit Imag.*, vol. 29, no. 2, pp. 216–225, Apr. 2016.
[42] R. Eswaraiah and E. S. Reddy, "Robust medical image watermarking technique for accurate detection of tampers inside region of interest and recovering original region of interest," *IET Image Process.*, vol. 9, no. 8, pp. 615–625, 2015.
[43] S. M. Mousavi, A. Naghsh, A. A. Manaf, and S. A. R. Abu-Bakar, "A robust medical image watermarking against salt and pepper noise for brain MRI images," *Multimedia Tools Appl.*, vol. 76, no. 7, pp. 10313–10342, Apr. 2017.
[44] S. A. Parah, J. A. Sheikh, F. Ahad, N. A. Loan, and G. M. Bhat, "Information hiding in medical images: A robust medical image watermarking system for E-healthcare," *Multimedia Tools Appl.*, vol. 76, no. 8, pp. 10599–10633, Apr. 2017.

[45] A. Sharma, A. K. Singh, and S. P. Ghrera, "Robust and secure multiple watermarking for medical images," *Wireless Pers. Commun.*, vol. 92, no. 4, pp. 1611–1624, Feb. 2017.
[46] F. N. Thakkar and V. K. Srivastava, "A blind medical image watermarking: DWT-SVD based robust and secure approach for telemedicine applications," *Multimedia Tools Appl.*, vol. 76, no. 3, pp. 3669–3697, 2017.
[47] R. Ahmed, B. Hassan, and B. Li, "Robust hybrid watermarking for security of medical images in computer-aided diagnosis based telemedicine applications," presented at the IEEE Int. Symp. Signal Process. Inf. Technol. (ISSPIT), Dec. 2018.

BILAL HASSAN received the B.S. degree in telecommunication engineering from Foundation University, Islamabad, Pakistan, in 2013, and the M.S. degree in electrical engineering from the University of Engineering and Technology (UET) Taxila, Taxila, Pakistan, in 2016. He is currently pursuing the Ph.D. degree in pattern recognition and intelligent systems with Beihang University, Beijing, China.

He was a Research Assistant with UET Taxila, from 2014 to 2016. From 2015 to 2016, he was a Management Associate with Pakistan Telecommunication Corporation Limited (PTCL), Pakistan. He is on study leave for his Ph.D. degree from National Telecommunication Corporation (NTC), Pakistan, where he was an Assistant Divisional Engineer. His research interests include the domain of retinal imaging, medical image processing, communication, and control systems. He was a recipient of the Chinese Government Scholarship (CGS) for pursuing his Ph.D. studies. He has also been a regular Reviewer of IEEE Access.

RAMSHA AHMED received the B.E. degree in telecommunication engineering and the M.S. degree in information security from the National University of Sciences and Technology (NUST), Islamabad, Pakistan, in 2013 and 2017, respectively. She is currently pursuing the Ph.D. degree in information and telecommunication engineering with the University of Science and Technology Beijing (USTB), Beijing, China. Her research interests include medical image processing, information security, the IoT, and machine vision-related applications.

BO LI received the B.S. degree in computer science and engineering and the M.Sc. degree in computer system structure from Xian Jiaotong University, Xi'an, China, in 1996 and 1999, respectively, and the Ph.D. degree in computer science from the University of Essex, in 2004.

He has been with the School of Computer Science and Engineering, Beihang University, since 2005. His main research interests include computer architecture, artificial intelligence, HPC, and related applications.

OMAR HASSAN received the B.S. degree in electrical engineering from the Center for Advanced Studies in Engineering (CASE), Islamabad. His research interests include the area of machine learning, computer vision, embedded systems, and intelligent machines.